Journal of Inflammation Research

Dovepress
Taylor & Francis Group

Open Access Full Text Article

ORIGINAL RESEARCH

Sirp-α Antibody Inhibits Renal Cell Carcinoma Progression via Akt1/Akt2 Modulation in Tumor-Associated Macrophages

Junfeng Hao[1,2,*], Naiquan Liu[3,*], Xin Huang[1,*], Hanlei Zhou[3], Hanrong Li[4], Yizhou Zhang[4], Bing Yu[5], Ziqian Bi[6], Xinyuan Song[7], Shunan Li[8], Keyu Chen[9], Ning Li[10], Chao Zhu[11], Jiahe Wang[1]

[1]Department of Family Medicine, Shengjing Hospital of China Medical University, Shenyang, People's Republic of China; [2]Department of Nephrology, and Guangdong Provincial Key Laboratory of Autophagy and Major Chronic Non-Communicable Diseases, Affiliated Hospital of Guangdong Medical University, Zhanjiang, People's Republic of China; [3]Department of Nephrology, Shengjing Hospital of China Medical University, Shenyang, People's Republic of China; [4]Department of General Surgery, Shengjing Hospital of China Medical University, Shenyang, People's Republic of China; [5]Department of Medical Imaging, Shengjing Hospital of China Medical University, Shenyang, People's Republic of China; [6]Faculty of Information Technology, Beijing University of Technology, Beijing, People's Republic of China; [7]School of Physics, Peking University, Beijing, People's Republic of China; [8]BeeMI, Saint Louis, MO, USA; [9]Georgia Institute of Technology, GA, USA; [10]Yuqing Hemodialysis Service Management Group Co., Ltd, Shenyang, People's Republic of China; [11]Department of Rheumatology and Immunology, The Third Affiliated Hospital of Naval Medical University, Shanghai, People's Republic of China

*These authors contributed equally to this work

Correspondence: Chao Zhu, Department of Rheumatology and Immunology, The Third Affiliated Hospital of Naval Medical University, Shanghai, 201805, People's Republic of China, Email zhuchaokidney@163.com; Jiahe Wang, Department of Family Medicine, Shengjing Hospital of China Medical University, Shenyang, 110022, People's Republic of China, Email wangjh1@sj-hospital.org

Introduction and Aim: Immunotherapies targeting tumor-associated macrophages (TAM) to improve antitumor immunity, are promising treatment strategies for many types of cancer. The signal-regulatory protein-α (Sirp-α)/CD47 axis is a key innate immune checkpoint target important in regulating phagocytosis in macrophages. We aimed to determine whether a Sirp-α monoclonal antibody (mAb) could prevent renal cell carcinoma (RCC) progression by acting on macrophages and modifying their phenotype.

Methods: We explored the gene expression signature of macrophages in the RCC microenvironment by analyzing transcriptome data of blood monocytes from patients with RCC vs healthy donors, and macrophages vs non-immune cells in RCC from public databases. We characterized the prevailing macrophage polarization phenotypes and the different ratios of Akt1 and Akt2 in RCC according to cell surface markers and expression profiles, prior to examining the effect of Sirp-α mAb on the M2 macrophage polarization in an in vitro co-culture model of RCC cells with macrophages. The co-culture model included human RCC cell lines and induced M2 macrophages, including a subset that had been transfected to overexpress phosphoinositide 3-kinase (PI3K).

Results and Conclusion: Treatment of RCC with Sirp-α mAb counteracted the enhanced migration and invasion of RCC as measured in wound healing and transwell assays and in vivo model. Collectively, our data showed that the different ratio of Akt1 and Akt2 of the PI3K/Akt pathway is involved in the RCC-induced M2 polarization of macrophages and that a new mechanism that the Sirp-α mAb inhibited M2 macrophage polarization by regulating components of the PI3K/Akt pathway. Elucidating the mechanism by which Sirp-α mAb inhibits the development of RCC allows us to provide a new theoretical basis for the study of the mAb in RCC immunotherapy.

Keywords: Sirp-α, renal cell carcinoma, macrophage, immune checkpoint, PI3K/Akt pathway

Introduction

Kidney cancer is one of the ten most common cancers and has an increasing incidence rate.[1] Renal cell carcinoma (RCC) is the most common form of kidney cancer, accounting for >80% of all kidney cancer cases.[2,3] Although existing tumor-targeted drugs have been used for the treatment of incurable metastatic RCC, their therapeutic effects are unsatisfactory[4–6] for accompanying by varying degrees of distant organ metastasis,[7] and the systemic surgery is a primary modality in treatment.

Received: 27 March 2025
Accepted: 10 September 2025
Published: 1 October 2025

Graphical Abstract

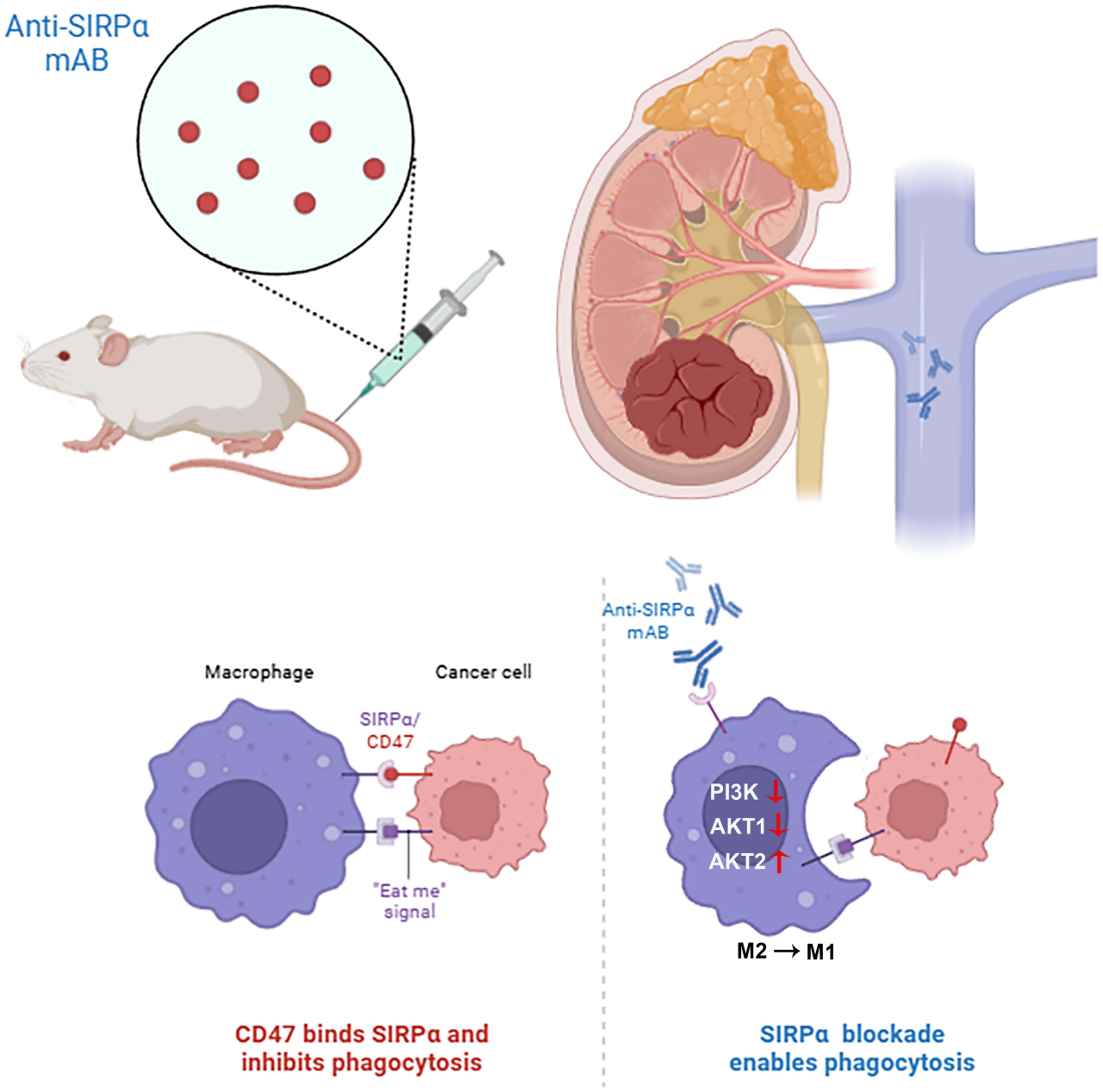

More recently, immunotherapies that target the antitumor response of the innate immune system, or checkpoint inhibitors, have proved useful as anticancer agents.[8,9] For example, studies conducted in a mouse model have shown that melanoma and RCC tumor formation are reduced upon treatment with antibodies against an inhibitory immune checkpoint receptor, the signal regulatory protein (Sirp)-α, which is expressed on myeloid cells, including macrophages.[10]

Macrophages are derived from monocytes and have key roles in immune surveillance and the maintenance of tissue homeostasis; these functions are primarily mediated through the phagocytosis of cellular debris and foreign substances,[11–13] including tumor cells.[14] Phagocytosis is tightly controlled, with macrophage receptors that recognize ligands on potential targets that are prophagocytic, signaling "eat me", or inhibitory, signaling "don't eat me".

Macrophages can adopt various phenotypes between two extremes: classically activated macrophages (M1) and alternatively activated macrophages (M2).[15] Recruitment of macrophages into the tumor microenvironment can promote their polarization into cancer-supporting, immunosuppressive tumor-associated macrophages (TAMs).[16,17] TAMs, primarily M2 macrophages, that infiltrate malignant metastatic cancers do not engulf tumor cells but instead help tumor cells escape death and promote tumor growth and metastasis.[18,19] Immunotherapies targeting TAMs thus hold great potential as adjunctive cancer treatments.[20,21]

Akt (also known as PKB) is a family of three serine/threonine protein kinases (Akt1, Akt2, and Akt3) that regulate a host of cellular functions, including cell survival, proliferation, differentiation, and intermediary metabolism. Previous studies demonstrate that Akt2 ablation results in the M2 polarization of macrophages, whereas Akt1 ablation promotes their M1 polarization,[22,23] which means, by inhibiting individual Akt isoforms, we may be able to modulate innate immunity and inflammation.

Tumor cells can evade immune surveillance by interacting with immune cells such as macrophages and T-lymphocytes through cell type-specific pathways.[24–26] Elevated CD47 expression in some cancers is associated with decreased survival and limited clearance by phagocytes expressing the CD47.[27] The Sirp-α/CD47 axis constitutes a key innate immune checkpoint that allows tumor cells to escape macrophage-dependent phagocytosis.[20] Sirp-α has a limited expression pattern and is primarily expressed in macrophages, dendritic cells, and neutrophils. When bound to its ligand, CD47 which is expressed on the surface of normal and tumor cells, Sirp-α recruits protein tyrosine phosphatases to inhibit the triggering of phagocytosis. Targeting this immune checkpoint using anti-CD47 or anti-Sirp-α agents to block the interaction between CD47 on tumor cells and Sirp-α on macrophages has become a promising cancer immunotherapy strategy, through augmented phagocytic activity mediated by as yet unclear mechanisms,[8,9] is worth further exploring in depth.

A previous study has shown that anti-Sirp-α monoclonal antibodies (mAb) markedly suppress RCC tumor formation in immunocompetent syngeneic mice;[10] however, the detailed effects of anti-Sirp-α antibody on TAM phenotype and the mechanisms of the antitumorigenic action have not been described. The aim of this study was to examine the effects of a Sirp-α mAb on macrophages in RCC cell lines and a mouse model and investigate the mechanisms underlying the anticancer effects.

Materials and Methods

Patient Samples and Ethical Statement

In this research, twenty matched renal cell carcinoma (RCC) tumor specimens, their respective neighboring non-cancerous tissues, and 40 blood samples were procured from RCC patients at the Shengjing Hospital of China Medical University. The investigation adhered to the Declaration of Helsinki's guidelines and received approval from the ethics committee of the Shengjing Hospital of China Medical University (Ethical Lot Number: 2023PS339K). All study participants provided informed consent, and patients submitted written informed consent for the publication of this manuscript.

Bioinformatic Analysis

The Gene Expression Omnibus (GEO) repository of the National Center for Biotechnology Information (NCBI; https://www.ncbi.nlm.nih.gov/) was searched for gene expression datasets from macrophages and other non-immune cells, and the RCC dataset GSE84697 belonging to the biological project PRJNA330854. SRR3942967, SRR3942973, SRR3942974, SRR3942975, and SRR3942976 and five public FASTQ files were then extracted from PRJNA330854. Public FASTQ files were downloaded from the European Nucleotide Archive (https://www.ebi.ac.uk/ena). Trim Galore (v0.6.5–1; https://www.bioinformatics.babraham.ac.uk/projects/trim_galore/) was used to trim the original sequence and FastQC and MultiQC software (version 1.9) were used to obtain the gene quality control report. Raw sequence reads were aligned to the human genome hg19 using Subjunc (v2.0.1). The gene expression level was quantified using featureCounts (v2.0.1) based on the GENCODE gene model version release 19 (GRCh37.p13), and the expression matrix was obtained. A separate analysis of gene expression in blood myelomonocytic cells from the RCC patient dataset was performed using GSE38424.

The analysis of the expression matrix was conducted through intergroup examination and principal component analysis (PCA) ($P < 0.05$). The prediction of differentially expressed genes was performed using a linear model analysis

with the Bioconductor package "DESeq2". The "fgsea" R package was employed to perform Gene Set Enrichment Analysis (GSEA) on the entire set of differentially expressed genes (DEGs), and the Genomes (KEGG) metabolic pathway enrichment analyses were carried out using the Bioconductor package "clusterProfiler" to obtain the key pathway information with the outcomes visualized using R language.

Cell Culture

The human RCC cell lines (ACHN) and mice renal cell lines (Renca) from the American Type Culture Collection (Manassas, VA, USA) were cultured in Dulbecco's modified Eagle's medium (DMEM; Biological Industries, Shanghai, China) supplemented with 10% fetal bovine serum (FBS, Biological Industries, USA), penicillin (100 U/mL), and streptomycin (100 g/mL). All cells were cultured at 37°C in an incubator with a humidified atmosphere containing 5% CO_2. For the $CD47^-$ ACHN cells, we transfected the si-CD47 small interfering RNA into ACHN cell lines for 24 h and acquired the ACHN cells.

THP-1 cells (human acute monocytic leukemia cell line) from the American Type Culture Collection (Manassas, VA, USA) were cultured in Roswell Park Memorial Institute (RPMI) 1640 medium (Gibco by Life Technologies, Grand Island, NY) supplemented with 10% heat-inactivated FBS and 0.05 mM 2-mercaptoethanol at 37°C in a 5% CO_2 incubator. Macrophages were obtained after 72 h of culture in RPMI 1640 medium supplemented with 80 nM phorbol 12-myristate 13-acetate (PMA). Macrophages were polarized to the M2 state by stimulation with lipopolysaccharide (LPS; HY-D1056, 50 ng/mL, Med Chem Express, USA) and interleukin-4 (IL-4; HY-108688, 20 ng/mL, Med Chem Express). For experimental purposes, the cells were divided into four groups: M2 groups, M2 + PI3K groups (the PI3K over-expressed groups: Lenti-PI3K was added at the beginning of the stimulation), M2 + PI3K + Sirp-α groups (Sirp-α mAb was added at a concentration of 10 μg/mL to the cells after transferred Lenti-PI3K), and M2 + Sirp-α groups (Sirp-α mAb was added at a concentration of 10 μg/mL to the cells). Sirp-α mAb was synthesized by Biotech Co., Ltd.[8] All experimental groups were cultured in quadruplicate. After 24 h of induction, the samples were collected for RNA extraction and qRT-PCR or protein extraction and Western blot analysis.

Co-Culture System

To verify the effect of tumor cells on macrophage phenotype, we collected conditioned medium (CM) of ACHN cells. And the macrophages were exposed to the different disposal of the CM of the ACHN cells for 24 h. And to verify the mechanism of Sirp-α mAb in RCC, we co-cultured the ACHN cell lines with the CM under the different disposal of the M2 macrophages for 24 h.

Immunofluorescence Studies

A fluorescein-labeled antibody was used to detect the corresponding antigen in the patients kidneys tissues. The corresponding primary antibodies were Akt1 (1:500, ab81283, Abcam, Cambridge, London, UK), Akt2 (1:500, ab175354, Abcam, Cambridge, London, UK), Ki-67 (1:500, ab15580, Abcam, Cambridge, London, UK), CD68 (1:500, ab254579, Abcam, Cambridge, London, UK), CD206 (1:500, CST, #24595, Boston, USA). PBS (0.01 mol/L, pH7.4) was replaced every 10 min to maintain specimen humidity. The specimen was covered with fluorescent-labeled antibodies and placed in an enamel box for 30 min. Excess moisture was subsequently absorbed from the glass slide, and a drop of glycerol was added to cover the glass before visualizing under a fluorescence microscope.

Transwell Assay

Transwell invasion and migration tests were conducted in 24-well plates (Corning, CLS33778, USA) utilizing a 6.5-mm diameter transwell chamber equipped with 8-mm transwell inserts. The ACHN cells (5×10^4) were suspended in 200 mL of serum-free DMEM medium and placed at the base of the upper chambers for migration experiments. Medium containing 10% FBS was introduced to the lower chamber. For invasion assays, the insert membranes were pre-coated with Matrigel (50 mL/well) (BD Biosciences) prior to cell addition. Following a 24-hour incubation, cells were stained with 0.1% crystal violet for 30 minutes, and non-migratory or non-invasive cells were removed through washing. The number of migrated cells was determined by randomly selecting six visual fields.

Wound Healing Assay

The ACHN cells were exposed to macrophage cell-conditioned medium, either with or without it, for a duration of 24 hours. Subsequently, the RCC cells were collected and placed in a 6-well plate, with a concentration of 2×10^5 cells per well. Using a sterile 200 μL pipette tip, a scratch wound was created, and any floating cells were eliminated by rinsing with 1x PBS. At 0 and 24 hours post-scratch, images of the wounds were taken using a Nikon Inverted Research Microscope Eclipse Ti at a magnification of 100×.

RNA Extraction and Quantitative Real-Time PCR

Total RNA was isolated from cells using TRIzol reagent (Takara, RR820A, China), according to a standard protocol. RNA was converted to cDNA using a TaKaRa reverse recording kit (Takara, RR047A, China). The 7900HT Quick Real-time PCR System (Applied Biosystems, Foster City, CA, USA) and SYBR Premix EX Taq were used to analyze mRNA expression, and the primer sequences used were listed in Supplementary Table 1.

Extraction of Total Protein and Immunoblotting Analysis

The complete protein extracts were obtained by utilizing RIPA lysis buffer (Beyotime, P0013B, China), which involved a sequence of incubation, vortexing, and centrifugation (15,000 ×g, 4°C for 25 min). Protein concentrations were determined using the BCA reagent (Beyotime, ST2222-25 g). The total protein was then separated via SDS-PAGE (100 V, 1.5 h) and subsequently transferred to polyvinylidene difluoride membranes (Millipore, USA) (50 V, 80 min). Following a 1-hour blocking period in 5% nonfat milk, the membranes were incubated overnight at 4°C with the specified primary antibodies: anti-PI3K (1:1000, CST, #4292, America), anti-p-PI3K (1:1000, CST, #17366, America), anti-Akt1 (1:1000, Abcam, ab314110, UK), anti-Akt2 (1:1000, Abcam, ab131168, UK), anti-E-cadherin (1:1000, Abcam, ab76055, UK), anti-N-cadherin (1:1000, Abcam, ab76011, UK), anti-Vimentin (1:1000, Abcam, ab20346, UK), IL-10 (1:1000, Abcam, ab215975, UK), Arg1 (1:1000, Abcam, ab133543, UK), and anti-β-actin (1:1000, Abcam, ab8226, UK).

Measurement of Cytokine Production

The concentrations of cytokines in the serum of patients and controls were analyzed using commercial ELISA kits (ElabScience, Houston, TX), specific for human IL-4 (E-EL-H0101c), IL-10 (E-EL-M0046c), TGF-β (E-EL-0162c), IL-1 (E-MSEL-M0003), IL-6 (E-EL-H6156), IL-12 (E-EL-H0150c), and TNF-α (E-EL-H0109c). These were used to detect the cell culture supernatants. All experiments were performed in accordance with the manufacturer's protocol.

Flow Cytometry

The macrophage cells exposed with the condition medium of the ACHN cells were washed with the PBS and stained with surface antibodies and a fixable viability dye. The antibodies used in flow cytometry analysis included CD86 (BD Biosciences, 555660, CA, USA) and CD206 (eBioscience, PE-CD206, San Diego, CA, USA). After transfection, cells (1×10^6) were harvested and mixed with the antibodies in 1 × Binding Buffer for 30 min at 37°C in the dark. Flow cytometry was performed using a Becton Dickinson FACSCalibur flow cytometer (San Jose, CA, USA). Data were analyzed using FlowJo 10.4.2 software (BD Biosciences).

Macrophages Killing Assay

Anti-$CD86^+$/$CD206^+$ and IL-4 activated $CD206^+$ macrophage cells were co-cultivated with cancer cells for a 24 h. According to the instructions of the Caspase-3/7 green detection reagent (Invitrogen) for cell apoptosis detection, count the total number of cells and the number of apoptotic cells stained with green fluorescence under a fluorescence microscope to calculate the percentage of surviving cells.

In vivo Metastasis Assessment

For the metastasis model, male NSG mice (6 weeks old) were utilized in accordance with the Guiding Opinions on the Treatment of Laboratory Animals and the Laboratory Animal Guideline for Ethical Review of Animal Welfare, as

prescribed by the National Standard GB/T35892-2018 of the People's Republic of China. All procedures involving mice were approved by the China Medical University Standards for Laboratory Animals Welfare and Ethical Review (Ethical Lot Number: KT2022256). The function of RCC-induced macrophages and the Sirp-α mAb in RCC (ACHN) metastasis was investigated by transducing ACHN cells (1×10^6) with a lentiviral luciferase vector (n = 3 per group) and co-injecting them with conditioned macrophage cells stimulated by Sirp-α mAb following the designated treatment. The cells were then introduced into the mice via tail vein injection to monitor distant metastasis. Bioluminescence was observed and documented on a weekly basis. After approximately four weeks, mice were intraperitoneally injected with 1.5 mg/10 g body weight D-luciferin. Ten minutes post-injection, representative bioluminescence images of metastases were captured using a Xenogen IVIS 200 Lumina Imager (Perkin Elmer, USA). Data acquisition and analysis were conducted using Living Image ver. 2.6 (Xenogen) software.

In vivo Xenograft Experiment and Biosafety Evaluation

We constructed a tumor model by injecting Renca cells (1×10^6 in 100 μL PBS) into the right side of the backs of BALB/c mice subcutaneously (Ethical Lot Number: 2024PS1672K). Ten days after Renca injection, PBS or Sirp-α mAb was dissolved in isotonic saline and 100 μL aliquots (corresponding to 2.5 mg/kg/day) were intraperitoneally injected into the tumor-bearing BALB/c mice. During the experimental period, the weight and tumor volume of the Renca cells in BALB/c mice were examined. Seven days after daily PBS or Sirp-α mAb injection, the animals were anesthetized and the tumor tissues were fixed and blood samples were collected for hematological and biochemical analysis, and major organ tissues were histopathologically analyzed using H&E staining.

Data Analyses

Statistical analyses were conducted using IBM SPSS software version 23.0 (IBM Corp., Armonk, NY). Data are presented as mean ± standard deviation (SD) or median with interquartile range, as appropriate. Differences between groups were assessed using the Student's *t*-test. A *P*-value of <0.05 was considered statistically significant.

Results

Sirp-α Inhibited the Tumor Growth and the Infiltration of M2 Macrophages

The biosafety of mAb is the primary concern. Therefore, we first evaluated the biocompatibility of the Sirp-α, such as the weight, blood biochemical indicators, organ pathological changes were evaluated to assess the biocompatibility of Sirp-α. First, we observed that there was no difference of the weight between the subcutaneous tumor-bearing mice treated with the PBS and Sirp-α mAb (Figure 1A). From the pathological sections of the main organs, no obvious pathological changes were detected after injecting each experimental group (Supplementary Figure 1A). Then, we detected the changes in several common indicators reflecting liver, kidney function, myocardial injury, and inflammatory reaction, including red blood cells (RBC), white blood cells (WBC), hemoglobin (HGB), platelet (PLT), creatinine (CREA), blood urea nitrogen (BUN), aspartate aminotransferase (AST), alanine aminotransferase (ALT), albumin (ALB), alkaline phosphatase (ALP). The results showed that there were no significant changes in the hematological and biochemical index, indicating that each experimental group would not cause liver, kidney, and inflammatory reaction (Supplementary Figure 1B–K). The above results showed that the Sirp-α had good biocompatibility and biosafety.

Next, we assessed the anti-tumor effects of Sirp-α mAb in the mice. For individual tumor growth, we observed a single explosive tumor growth in mice in the PBS. In contrast, tumor growth in the Sirp-α mAb treatment group was significantly reduced (Figure 1B). Meanwhile, we used the confocal microscopy to detect the expression of F4/80 and CD206 (two markers of M2-TAM) by IF assays of the tumor tissues, and we found Sirp-α mAb could significantly inhibited the M2 macrophages (Figure 1C). Then, we found that there were more M2 macrophages (CD68 and CD206, the two markers of M2-TAM of human) in the RCC of the patients than the adjacent healthy tissues (Figure 1D). In addition, we also found that the gene levels of CD206, CD163 and Arg-1 (M2 markers) were higher of the RCC than the adjacent healthy tissues (Figure 1E–G). And the protein levels of anti-inflammatory factors IL-4, IL-10, and TGF-β which can promote tumor growth and metastasis, and are the characteristic of M2 macrophages, were significantly

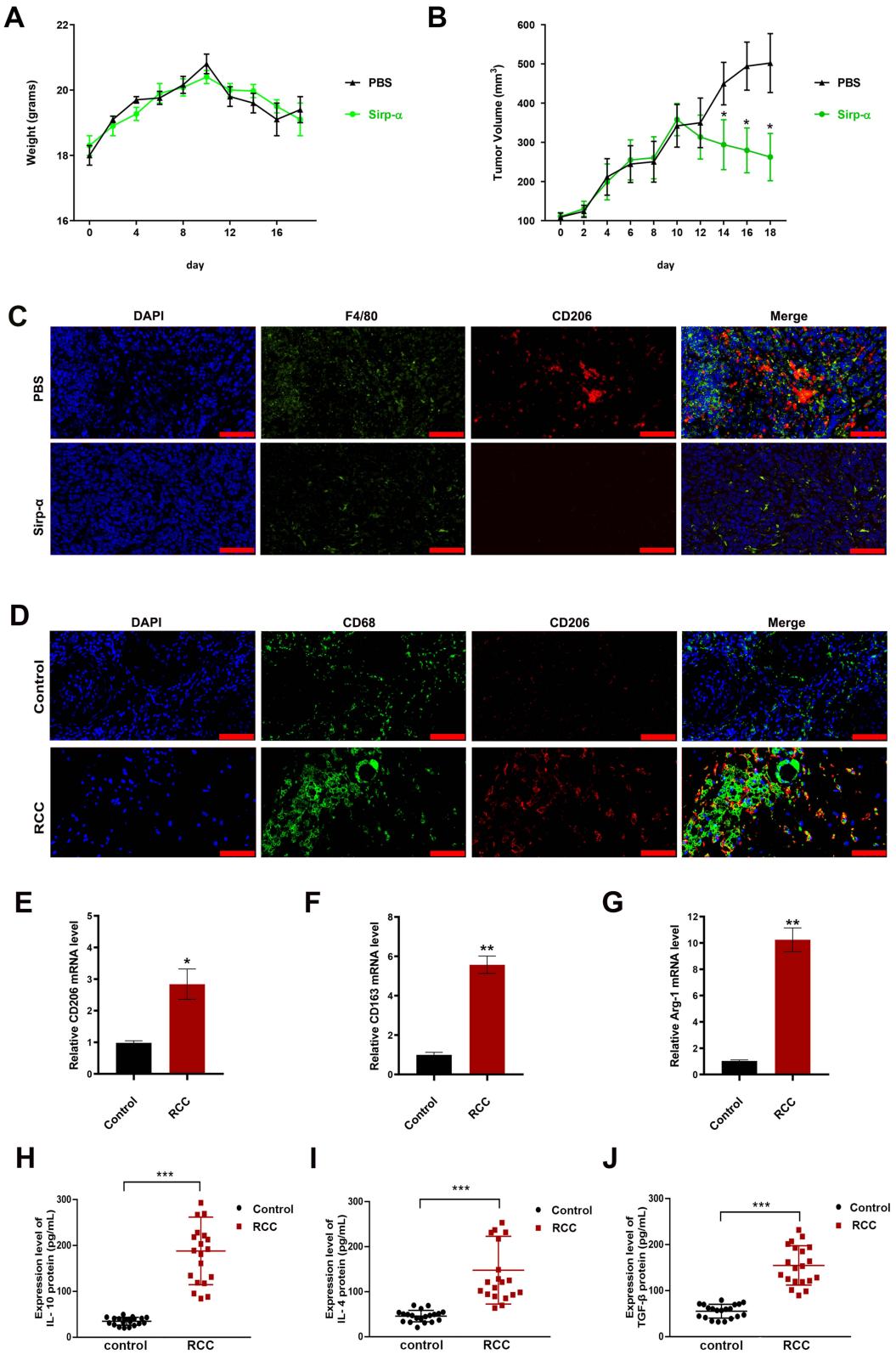

Figure 1 Antitumor activity of Sirp-α in vivo. (**A**) The body weight changes in tumor-bearing mice under different treatment. (**B**) The plot of overall tumor volume changes in tumor-bearing mice under different treatments.(**C**) Immunofluorescence co-localization by F4/80 (green fluorescence) and CD206 (red fluorescence) in mouse tumor tissues. Representative images are shown from a total of 3 animals per group. Values are shown as means±SD from three independent experiments. (**D**) Immunofluorescence co-localization by CD68 (green fluorescence) and CD206 (red fluorescence) in the RCC of patients and adjacent renal tissues. (**E–G**) The gene expression levels of M2-like macrophage markers (CD206, CD163 and Arg-1) in the RCC tissues and adjacent renal tissues by qRT-PCR. (**H–J**) The expression level of IL-10, IL-4, and TGF-β (markers of M2 macrophages) in the patients with RCC and the control group were analyzed using ELISA. (scale bar: 20 μm). Data are representative of three independent experiments. Values are shown as means±SD from three independent experiments. **P* <0.05, ***P* <0.01, ****P* <0.001.

https://doi.org/10.2147/JIR.S530775

upregulated in RCC (Figure 1H–J). These results suggested that the RCC microenvironment induced polarization of macrophages towards the M2 type, and Sirp-α mAb could alleviate the M2 macrophages expression and had the anti-tumor activity.

The Blood Monocytes of RCC Patients Exhibited a Protumor Expression Profile, and PI3K Pathway Activation

Blood monocytes and tumor-infiltrating monocytes affect the tumorigenesis and the tumor microenvironment.[20,28] To explore how the blood monocytes affect RCC of patients, we used data from public databases to compare the gene expression profiles of blood monocytes from patients with RCC and healthy donors. After comparing and enumerating the pruned gene expression data, we screened statistically significant DEGs using the Bioconductor package "DESeq2". Data analysis revealed a significant difference in blood monocyte gene expression profile between patients with RCC and healthy donors ($P < 0.05$). We found that 752 DEGs were upregulated and 952 were downregulated. The cutoff for logFC is 1.17 (Figure 2A–C). The results of GSEA pathway enrichment showed that the DEGs between the blood monocytes from patients with RCC and healthy donors were mainly enriched in endocrine resistance, antigen processing and presentation, and the progesterone-mediated oocyte maturation pathway. The genes enriched in these pathways included PIK3R2 (the regulatory subunit of PI3K) and MMP9 (tumor metastasis-associated enzyme) (Supplementary Table 2 and Figure 2D), which indicated that the gene expression profile of blood monocytes from patients with RCC exhibited a protumor transition, accompanied by the activation of the PI3K pathway.

PI3K is a Key Node Gene Shared by Pivotal GSEA Enrichment Pathways in Macrophages and Other Non-Immune Cells in RCC

To explore the gene expression signature of macrophages in the RCC microenvironment, we analyzed the transcriptome data of macrophages and non-immune cells in RCC using public databases. Our analysis revealed a significant difference between the $CD45^-$ non-immune cell and macrophage groups ($P < 0.05$). We found 643 genes were upregulated and 102 were downregulated (Figure 3A–C), and we have drawn a relationship diagram of the interactions between the upregulated DEGs in the Cnetplot through KEGG enrichment (Figure 3D), then we found the pathways of GSEA enrichment included bacterial invasion of epithelial cells, choline metabolism in cancer, Toll-like receptor signaling pathway, and alcoholism between the $CD45^-$ non-immune cell and macrophage groups of the RCC databases (Supplementary Table 3 and Figure 3E). Interestingly, we saw that PIK3CA (PI3K) was a key node gene that was shared by these pathways through GSEA and KEGG enrichment (Supplementary Table 4 and Figure 3F), which would imply that PI3K participants the macrophages of the immunoregulatory processes in the RCC.

The Different Ratio of Akt1 and Akt2 Modulated the Regulatory Genes Affecting RCC Associated Macrophages

In our further analysis, we found that there were different four kinds of expression of PI3K and Akt of the macrophages and $CD45^-$ non-immune cells in the RCC database. Akt1 and PIK3AP1 (PI3K) were expressed higher of the macrophages than the $CD45^-$ non-immune cells, while, Akt2 and Akt3 were expressed lower of the macrophages than the $CD45^-$ non-immune cells (Figure 4A). Next, we wanted to see if the RCC gene expression signatures and transcriptome data we had analyzed matched the molecular phenotypes of the macrophage populations in the RCC. We detected the expression of Akt1 and Akt2 in the macrophages of the RCC patients tissues. We selected the CD68 as the marker of macrophages of patients. The results showed that compared with the control tissues, there was more expression of Akt1 (Figure 4B) and less Akt2 (Figure 4C) of macrophages. Then, we analysed the DEGs between the two data sets through the Intersection Wayne diagram, and we found 25 up-regulated genes (CLEC7A, CSF3R, FCN1, MX2, CD244, TMEM71, GBP5, S100A12, RNASE2, CSTA, S100A9, ASGR2, CFP, PADI4, FXYD6, BANP, IRF7, MGAM, ADAM8, KLF2, FAM131A, SERPINB2, METRNL, P2RY1, TKTL1) and 1 down-regulated genes (FHL1) in the two data sets (Figure 4D). And we found the intersection genes were mainly enriched secretory granule lumen, cytoplasmic vesicle lumen, vesicle lumen, etc through the GO enrichment analysis and made the Cnetplot of the GO enrichment

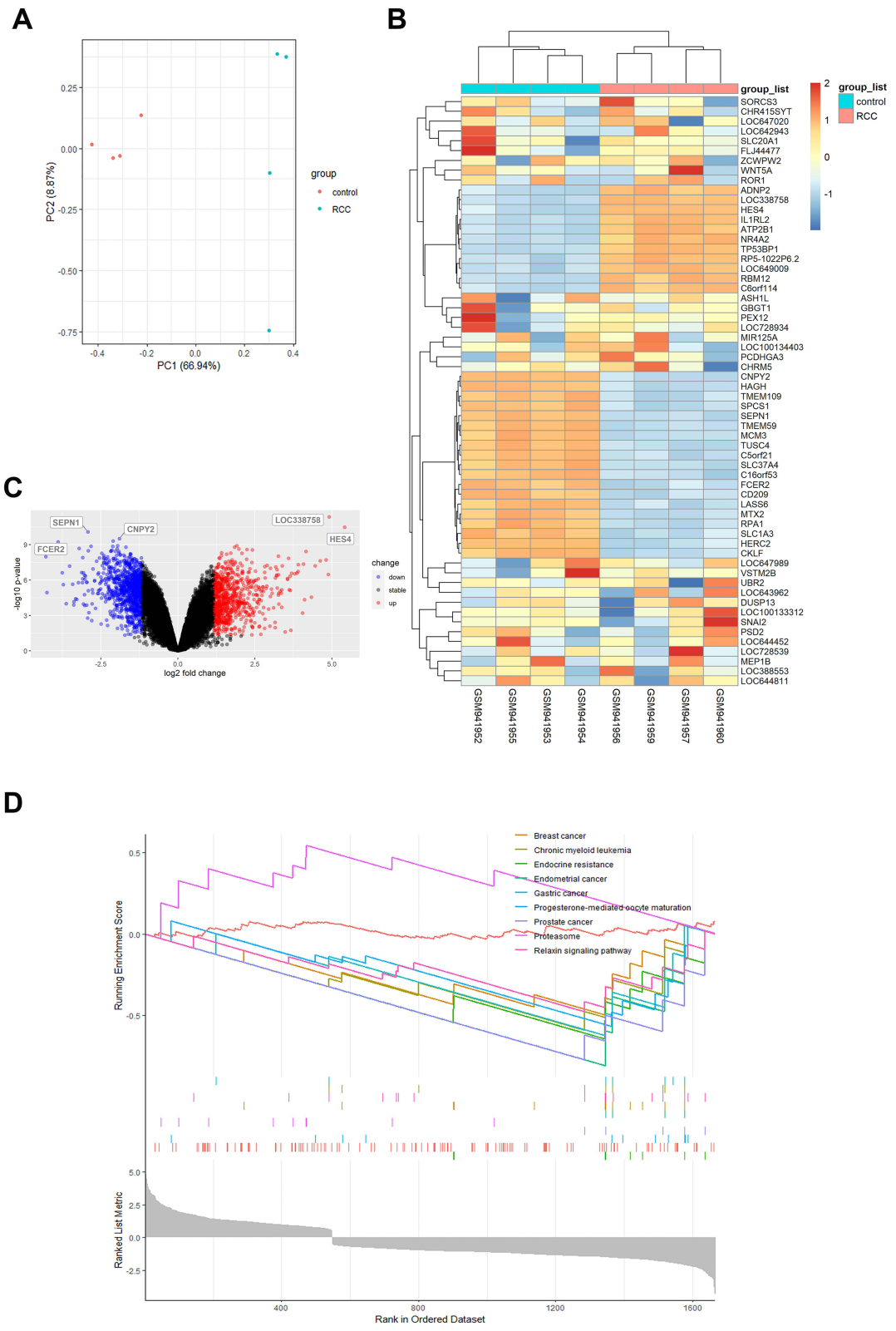

Figure 2 Gene expression profile analysis of blood monocytes from patients with RCC and healthy donors. (**A**) PCA of the gene expression in the blood myelomonocytic cells from patients with RCC and healthy donors. (**B**) Correlation of heatmap of differences between groups: a significant difference was observed between patients with RCC and healthy donors (P <0.05). (**C**) A total of 752 differentially expressed genes were upregulated and 952 differentially expressed genes were downregulated in the volcano plot. The cut-off for logFC is 1.17. (**D**) GSEA pathway enrichment showed the differentially expressed genes were mainly enriched in the endocrine resistance, antigen processing and presentation, and the progesterone-mediated oocyte maturation pathway.

https://doi.org/10.2147/JIR.S530775

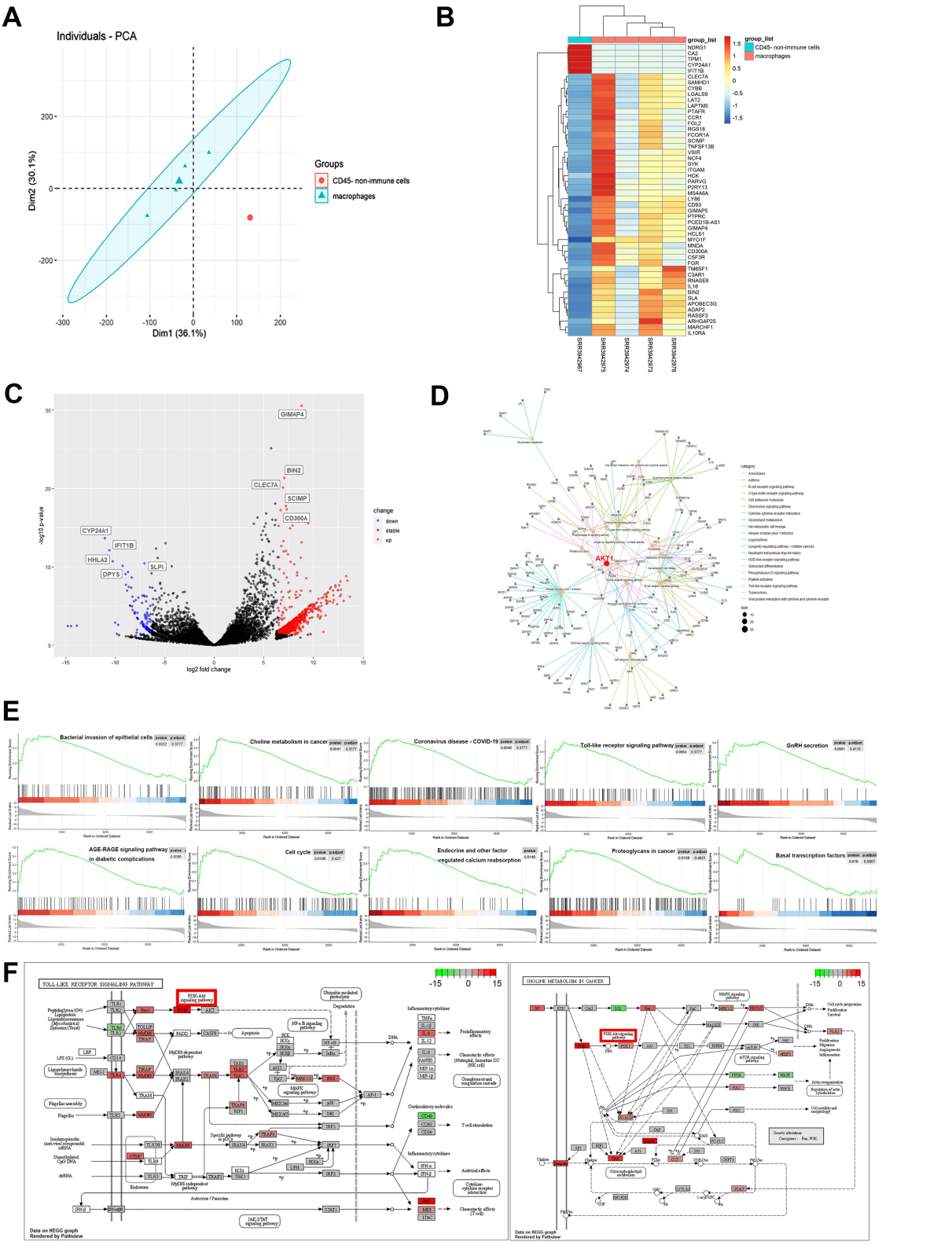

Figure 3 Gene expression profile analysis of macrophages and other non-immune cells in RCC. (**A**) PCA of the gene expression in the CD45 negative non-immune cell and macrophages groups. (**B**) Correlation of heatplot of differences between groups: a significant difference was observed between CD45 negative non-immune cell and macrophages groups in all differently expressed genes (P <0.05). (**C**) Differential gene volcano plot: 643 differentially expressed genes were upregulated and 102 differentially expressed genes were downregulated. The cut-off for logFC is 6.407. (**D**) Cnetplot of KEGG enrichment of upregulated genes. (**E**) GSEA pathway enrichment showed the differentially expressed genes were mainly enriched in the bacterial invasion of epithelial cells, choline metabolism in cancer, Coronavirus disease, Toll-like receptor signaling pathway, GnRH secretion, AGE-RAGE signaling pathway in diabetic complications, Cell cycle, and Endocrine and other factor-regulated calcium reabsorption and Proteoglycans in cancer. (**F**) The pivotal PI3K is the key node in these pathways of the KEGG enrichment such as the Toll-like receptor signaling pathway, bacterial invasion of epithelial cells and choline metabolism in cancer.

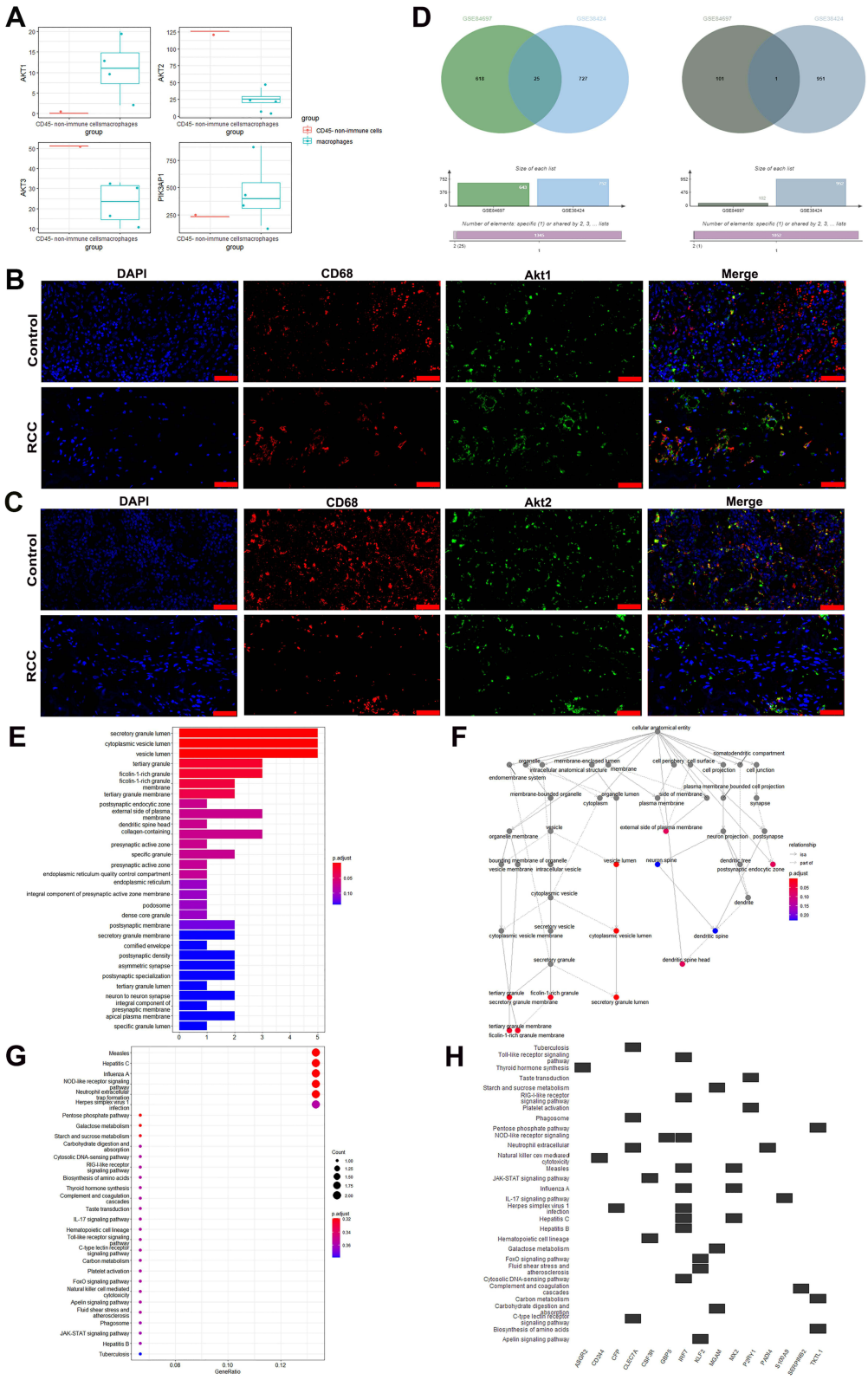

Figure 4 The different ratio of Akt1 and Akt2 modulated the regulatory genes affecting RCC associated macrophages. (**A**) Differential expression of PI3K and AKT in macrophages and other non-immune cells of RCC in boxplot. (**B**) Immunofluorescence co-localization by CD68 (red fluorescence) and Akt1 (green fluorescence) in the tumor tissues of the RCC patients. (scale bar: 20 μm) (**C**) Immunofluorescence co-localization by CD68 (red fluorescence) and Akt2 (green fluorescence) in the tumor tissues of the RCC patients. (scale bar: 20 μm). Data are representative of three independent experiments. Values are shown as means±SD from three independent experiments. (**D**) Intersection Wayne diagram of DEGs between the two data sets. (**E**) GO enrichment analysis of 25 up-regulated genes in the two data sets in the barplot. (**F**) Cnetplot of GO enrichment analysis. (**G**) KEGG enrichment analysis of 25 up-regulated genes in the two data sets in the dotplot. (**H**) Heatplot of KEGG enrichment analysis.

https://doi.org/10.2147/JIR.S530775

analysis (Supplementary Table 5, Figure 4E and F). Then, the KEGG enrichment analysis showed that the up-regulated intersection genes were enriched in NOD-like receptor signaling pathway, Pentose phosphate pathway, RIG-I-like receptor signaling pathway, etc, which participated in regulating the occurrence and development of tumors (Supplementary Table 6, Figure 4G and H). Therefore, we would explore whether Sirp-α mAb inhibits the tumorigenesis and progression of RCC by regulating the expression levels of Akt1 and Akt2 in macrophages.

Sirp-α mAb Inhibited RCC-Induced M2 Macrophage Polarization by Downregulation of the PI3K/Akt1 and Upregulation of Akt2

Firstly, we found the Akt1 and Akt2 were associated with the 25 up-regulated intersection genes and Sirp-α directly regulated PI3K (PIK3CA), Akt1 and Akt2 through the STRING database (Figure 5A and B). To explore whether the Sirp-α mAb can regulate M2 macrophage polarization in the RCC microenvironment, we tested its effect on the M2 macrophage polarization (the THP-1 cells induced with PMA and IL-4) under the conditioned medium of ACHN cells (Figure 5C). Contour plots from flow cytometry analysis of the frequencies of $CD206^+$ M cells demonstrated that RCC-conditioned medium (T-CM) markedly promoted the polarization of M2. As illustrated in Figure 5D, contour plots from flow cytometry analysis of the frequencies of the $CD86^+CD206^+$ M cells demonstrate that RCC markedly promoted the proliferation of M2. In contrast, the ratio of $CD206^+$ M2 cells reduced from 22.22% to 21.86% and there was more $CD86^+$ M1 cells (from 0% to 3.07%) after being disposed of with Sirp-α mAb. These results indicate that Sirp-α mAb treatment could alleviate M2 polarization and promote proinflammatory M1 phenotypic transformation in vitro. We then used macrophages killing assay to detect the killing ability of macrophages against tumors in a co-cultured system of the macrophages and the ACHN cells with different conditions. The results showed that compared with the ACHN+M groups, the macrophage with the dispose of the Sirp-α mAb killed more tumor cells, and the killing percentage was the highest after the ACHN cells knockdown CD47 (Figure 5E).

Then, we used the Western blotting to assess whether the Sirp-α mAb could affect the polarization of macrophages through the PI3K/Akt pathway. Firstly, we obtained M2 macrophages stimulated with PMA and IL-4. The results showed that the addition of the Sirp-α mAb decreased the levels of p-PI3K, and Akt1 and increased Akt2 compared with the M2 and M2+PI3K groups (Figure 5F and G). This finding indicated that the Sirp-α mAb inhibited the p-PI3K/Akt1 and promoted Akt2 expression. Furthermore, the PI3K overexpression (the group transferred with Lenti-PI3K) increased M2-like macrophage marker expression, including CD163, Arg1, and IL-10 while Sirp-α mAb treatment inhibited the expression of these markers (Figure 5H and I). Furthermore, we used qRT-PCR and ELISA to quantify the mRNA and proteins expression levels of M1 macrophage markers, proinflammatory factors IL-1, IL-6, IL-12, and TNF-α (Figure 5J and K). Here, we found that the Sirp-α mAb significantly increased their expression, indicating that the Sirp-α mAb promoted M1-like macrophage polarization and thus exerted proinflammatory effects. Collectively, the results showed that the Sirp-α mAb regulated the macrophage polarization by downregulating components of the PI3K/Akt1 and upregulating Akt2.

Sirp-α mAb Could Counteract the Enhanced Migration and Invasion of RCC-Induced by PI3K

To further elucidate whether the effect of the Sirp-α mAb on M2 polarization of RCC-induced macrophages can delay the development of RCC, we used a mixed culture model of macrophages (overexpressing PI3K or not) and RCC cells in vitro to determine the influence of Sirp-α mAb on RCC cell migration and invasion. We used the ACHN cell lines and M2 macrophages in the co-culture system (Figure 6A). In the wound healing and transwell assays (Figure 6B–D), we found that the overexpression of PI3K in macrophages could facilitate the migration and invasion of ACHN cells; however, the addition of Sirp-α mAb completely inhibited this effect. Additionally, we also demonstrated that the overexpression of PI3K in macrophages decreased the expression of E-cadherin (an epithelial cell marker) and increased the expression of N-cadherin and vimentin (a mesenchymal cell marker) by Western blotting; however, the addition of the Sirp-α mAb resulted in an almost complete offset of this phenomenon in ACHN cells (Figure 6E and F).

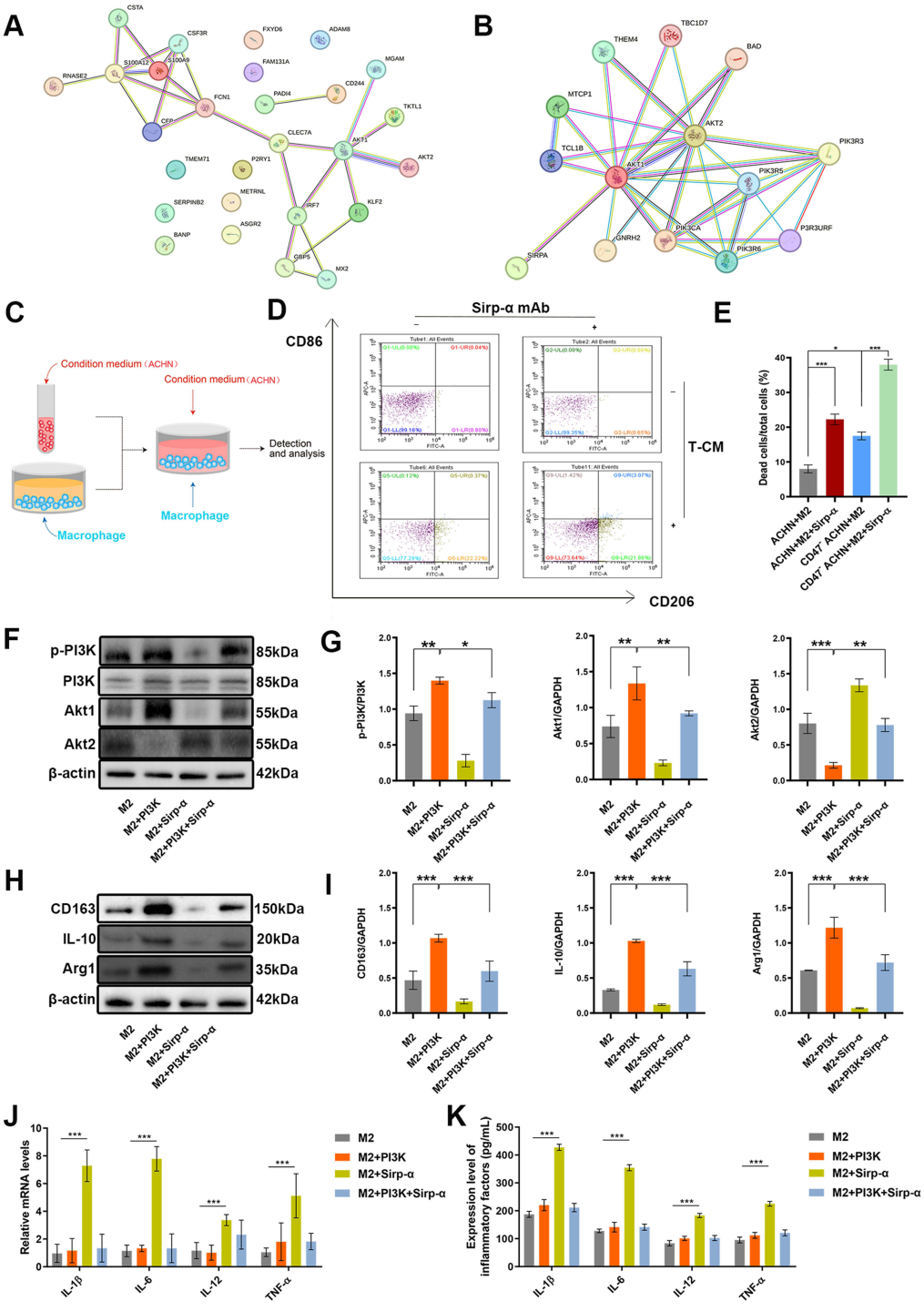

Figure 5 The Sirp-α mAb inhibited RCC-induced M2 macrophage polarization by regulation of the PI3K/AKT pathway. (**A**) The STRING mutual drawing of the Akt1 and Akt2 with the 25 up-regulated intersection genes. (**B**) The STRING mutual drawing of Sirp-α with PI3K, Akt1 and Akt2. (**C**) The co-cultivation mode diagram to test the effect of the tumor cells on the M2 macrophage polarization (the THP-1 cells induced with PMA and IL-4) in RCC cell line (ACHN)-conditioned medium. (**D**) Representative contour plots from flow cytometry analysis of the frequencies of the $CD206^{+}/CD86^{+}$ macrophages. (**E**) The macrophages killing assay to detect the killing ability of macrophages against tumors in a co-cultured system of the macrophages and the ACHN cells with different conditions. ACHN+M (the ACHN and macrophages co-cultured groups), ACHN+M+Sirp-α (Sirp-α mAb was added at a concentration of 10 μg/mL to the macrophages cells), $CD47^{-}$ACHN+M (the macrophages were co-cultured with the CM of the ACHN cells knockdown CD47), $CD47^{-}$ACHN+M+Sirp-α (the macrophages disposed with the Sirp-α mAb then were co-cultured with the CM of the ACHN cells knockdown CD47). (**F** and **G**) The protein expression of PI3K, p-PI3K, Akt1, Akt2 was detected using Western blotting and densitometric analysis. (**H** and **I**) The protein expression of M2 macrophage marker (CD163, Arg-1, and IL-10) expression in the four groups using Western blotting and densitometric analysis. (**J**) The qRT-PCR analysis of M1 macrophage marker (IL-1, IL-6, IL-12, and TNF-α) expression of the four groups. (**K**) The ELISA analysis of M1 macrophage marker (IL-1, IL-6, IL-12, and TNF-α) expression of the four groups. M2 groups (the isolate M2 cells groups), M2 + PI3K groups (the PI3K overexpressed groups: Lenti-PI3K was added at the beginning of the stimulation), M2 + Sirp-α groups (Sirp-α mAb was added at a concentration of 10 μg/mL to the cells) and M2 + PI3K + Sirp-α groups (Sirp-α mAb was added at a concentration of 10 μg/mL to the cells after transferred Lenti-PI3K). Data are representative of three independent experiments. Values are shown as means±SD from three independent experiments. **P* <0.05, ***P* <0.01, ****P* <0.001.

https://doi.org/10.2147/JIR.S530775

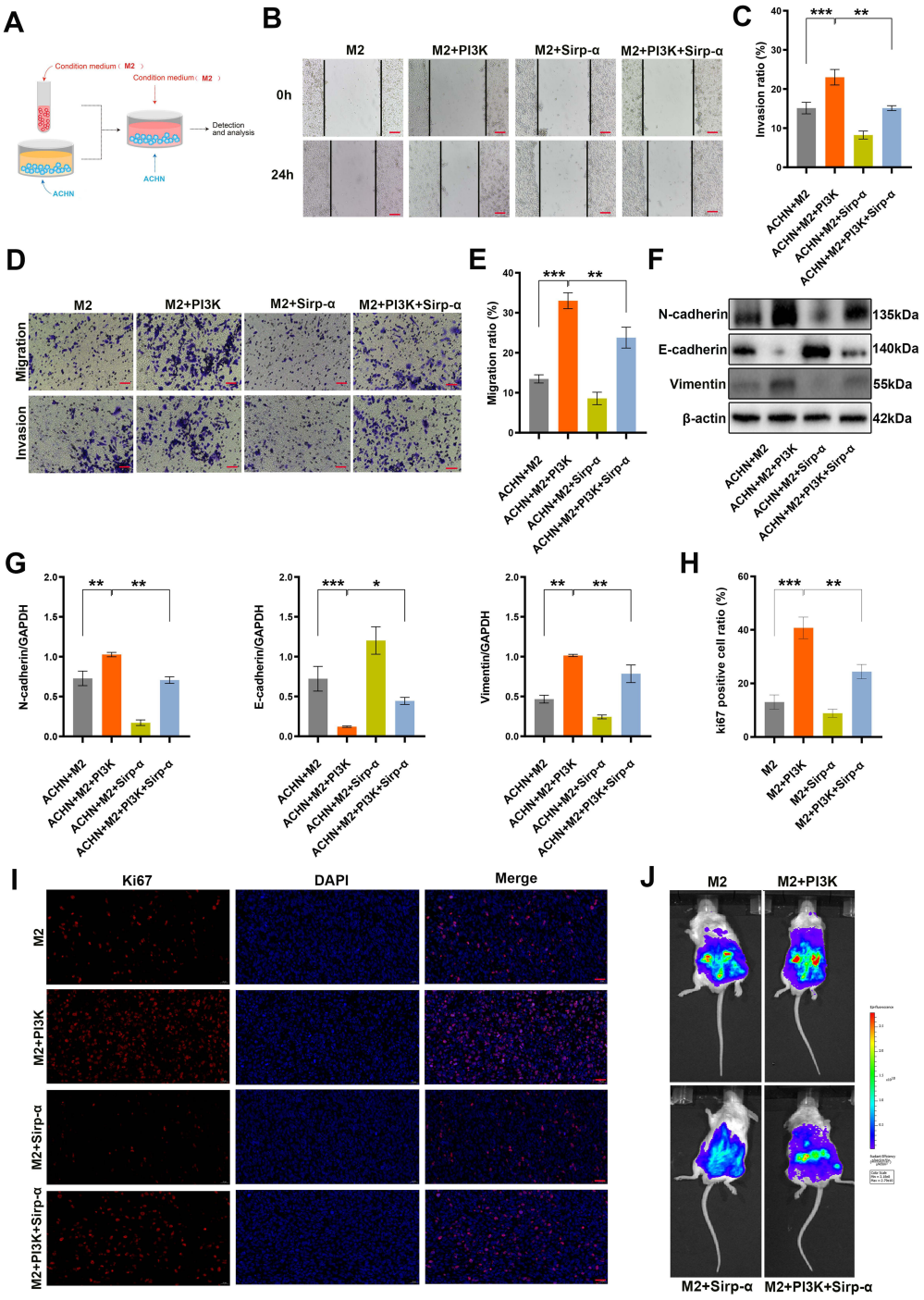

Figure 6 The Sirp-α mAb inhibited RCC cell migration and invasion *in vivo*. (**A**) The Co-cultivation mode diagram to test the effect of the M2 macrophage on the ACHN cells. (**B**) The scratch wound healing assays in ACHN cells (scale bar=100 μm). (**C** and **D**) Transwell assay to assess migration and invasion capacity of the ACHN cells treated with or without Sirp-α mAb and the statistical analysis (scale bar=100 μm). (**E** and **F**) Western blots and grey value of EMT-related protein expression in ACHN cells. ACHN + M2 groups (ACHN cells were exposed with the isolate M2 cells groups), ACHN + M2 + PI3K groups (Lenti-PI3K was added to the M2 at the beginning of the stimulation), ACHN + M2 + Sirp-α groups (Sirp-α mAb was added at a concentration of 10 μg/mL to the cells) and ACHN + M2 + PI3K + Sirp-α groups (Sirp-α mAb was added at a concentration of 10 μg/mL to the cells after transferred Lenti-PI3K). Data are representative of three independent experiments. (**G**) Immunofluorescence of Ki-67 (red fluorescence) in the mice tumor tissues. (scale bar: 20 μm). (**H**) Bioluminescence imaging of mice after cell injection into the tail vein. ACHN cells were co-injected with macrophages subjected to the indicated treatment. Metastasis was monitored and imaged by bioluminescence using an in vivo imaging system. M2 groups (the isolate M2 cells groups), M2 + PI3K groups (the PI3K overexpressed groups: Lenti-PI3K was added at the beginning of the stimulation), M2 + Sirp-α groups (Sirp-α mAb was added at a concentration of 10 μg/mL to the cells) and M2 + PI3K + Sirp-α groups (Sirp-α mAb was added at a concentration of 10 μg/mL to the cells after transferred Lenti-PI3K). (**I**) Immunofluorescence of Ki-67 (red fluorescence) in the mice tumor tissues. (scale bar: 20 μm). (**J**) Bioluminescence imaging of mice after cell injection into the tail vein. Metastasis was monitored and imaged by bioluminescence using an in vivo imaging system. Representative images are shown from a total of 3 animals per group. Values are shown as means±SD from three independent experiments. **P* <0.05, ***P* <0.01, ****P* <0.001.

Finally, we tested the effect of the Sirp-α mAb on RCC cell metastases using an in vivo subcutaneous tumor model and metastasis model. We could find the highest proliferation rate in the M2+PI3K group by detecting the expression of the cell proliferation marker Ki-67 through the IF assay of the tumor tissues. And it was significantly decreased in the Sirp-α mAb treated tumors (Figure 6G). Another, using a grouping approach similar to the in vitro assay described above, ACHN luciferase cells, and the conditioned M2 macrophages were injected into the tail veins of NSG mice. We used a live animal bioluminescence imaging system to monitor tumor metastasis on a weekly basis. We found that the overexpression of PI3K in macrophages could significantly enhance ACHN cell metastasis; however, Sirp-α mAb treatment could prevent this effect (Figure 6H). These results indicated that Sirp-α mAb exposure inhibited the RCC cell migration and invasion in an in vivo model.

Discussion

In our research, we treated macrophages with Sirp-α antibodies, so that after internalizing Sirp-α antibodies, macrophages did not express Sirp-α, and could not combine with CD47 and therefore, engulf cancer cells. We also found an interesting phenomenon that Sirp-α can reduce the Akt1 expression and promote the Akt2 expression, therefore, facilitate the M1 polarization and suppress M2 polarization in macrophages, significantly improved anti-cancer effect. Overall, we have revealed a new mechanism that the inhibitory effect of Sirp-α mAb treatment on M2-type macrophage polarization, which seemed to occur via PI3K/Akt pathway suppression, as indicated a potential scope for the further study.

Based on the analysis of transcriptome data of blood monocytes from RCC patients vs healthy donors and macrophages vs non-immune cells in RCC from public databases, we found that the RCC microenvironment has a considerable influence on the PI3K/Akt pathway in macrophages. We also demonstrated the inhibitory effect of the Sirp-α mAb on the expression of key components of this pathway. This study explored the application and underlying mechanism of this strategy in the context of RCC using THP-1 cells exposed with the conditioned medium of ACHN cells under different disposal environments. We showed that the overexpression of PI3K in macrophages could facilitate the migration and invasion of cells and the expression of N-cadherin and Vimentin and decreased the E-cadherin, and promoted the invasion and distant metastasis in cancer;[29–31] however, the addition of Sirp-α mAb completely inhibited this effect. And the Sirp-α mAb can reduce p-PI3K and Akt1 levels, promote Akt2 expression, indicating that Sirp-α mAb inhibits M2-like macrophage polarization by regulating components of the PI3K/Akt pathway. As previous studies have shown that PI3K/Akt pathway activation contributes to macrophage polarization,[32,33] Martina, et al, reported that the PI3K/Akt signal pathway strongly supports tumorigenesis and underscores the importance of isoform-specific Akt modulation in shaping TAM phenotypes and enhancing immunotherapy efficacy,[34] and Akt kinases differentially contribute to macrophage polarization, with Akt1 ablation giving rise to an M1 and Akt2 ablation resulting in an M2 phenotype.[35,36] This is consistent with our research content, in which we proposed a new mechanism of action of Sirp-α mAb, which affects the phenotype transition of macrophages by regulating the expression of Akt1 and Akt2, thereby inhibiting tumor progression.

CD47 is expressed in almost all cell types, CD47-targeting antibodies and inhibitors have been investigated in various preclinical and clinical trials. However, anemia and thrombocytopenia appear to be formidable challenges since CD47 is ubiquitously expressed on erythrocytes.[37] Therefore, from a security perspective, we choose Sirp-α instead of CD47. Sirp-α mainly expressed in the compartments of myeloid cells, including monocytes, macrophages, granulocytes, and DC subpopulations.[38] Block the interaction between CD47 and Sirp-α can promote the elimination of cancer cells in vitro and in vivo.[39] Previous studies have shown that the CD47 overexpression to disguise oneself is a common mechanism for cancer cells to evade immune surveillance and blocking CD47 or Sirp-α can eliminate the “don’t eat me” signal and allow macrophages to engulf.[40] Macrophages that infiltrate tumors can undergo modification within the tumor microenvironment from antitumorigenic M1 macrophages to protumorigenic M2 TAMs.[20,41] Inhibiting or reversing this transformation of macrophages and increasing the proportion of M1 macrophages in the tumor microenvironment are core strategies for maintaining the antitumor effect of macrophages.[21]

Sirp-α is expressed in macrophages, dendritic cells, and neutrophils, all of which participate in cancer immunology and metastasis.[8] Therefore, the Sirp-α mAb may target multiple myeloid cell subsets in the RCC microenvironment. Indeed, others have reported that an anti-human Sirp-α antibody enhances the antitumor activity of human neutrophils

and macrophages in vitro.[9] Whether the anti-Sirp-α mAb can target dendritic cells and regulate their antitumor effects, however, has not yet been reported.[42] The specific effects on neutrophils and dendritic cells of the administration of Sirp-α mAb and the elucidation of their role alongside macrophages is worthy of further study. In addition, Milena et al indicated Immune Checkpoint Inhibitors (ICI) lead to better outcomes (improved Overall survival rate (OS) and low tumour burden) and Cytoreductive nephrectomy + anti-VEGF and mTOR results in a significant improvement in mean OS compared to surgery alone.[7] Macrophages have good chemotaxis towards tumors, using macrophages as ICI is more beneficial for tumor killing, whether it is in situ cancer or metastatic cancer. Therefore, we have chosen macrophages as our primary research subject, and we will further expand the study of cell types in future research. Another, it has also been reported that the combination of anti-Sirp-α mAb and other anticancer antibodies, such as tumor-targeting Abs rituximab, cetuximab, and avelumab, could enhance phagocytosis and synergistically suppress tumor growth.[9] Exploring the potential synergistic effect and mechanism of the Sirp-α mAb combined with other anticancer antibodies in preventing the progress of RCC would be informative prior to using the Sirp-α mAb clinically to achieve ideal efficacy.

Although our research has revealed the antitumor activity of the Sirp-α mAb, however, it is unclear whether Sirp-α mAb exposure exerts this effect through a direct or indirect action, and the specific molecular target of the Sirp-α mAb that exerts this effect was not identified in the scope of this work. And the sample size did not reach the initially expected level due to practical limitations in vivo. We also need to study its effects on other phagocytic cells, downstream target molecules, and the effective mechanisms are warranted prior to progressing this promising treatment strategy into clinical practice further. Future work that includes spatial transcriptome sequencing and single-cell sequencing analysis based on appropriate in vivo models and needs to investigate the potential off-target effects of the antibody and measure of the signalling activity of the pathway may provide data for further elucidation of the detailed mechanisms.

In summary, our data support that the Sirp-α mAb can increase the ratio of M1 to M2 macrophages in RCC by inhibiting M2 macrophage polarization via downregulating the PI3K/Akt1 and upregulating Akt2 pathway, resulting in the reduction of the RCC migration and invasion, but whether the regulation is direct needs further clarification. We have thus developed a preliminary elucidation of the antitumor mechanism of the Sirp-α mAb-in RCC treatment.

Data Sharing Statement

The datasets generated and/or analyzed during the current study are available from the corresponding author (Dr Jiahe Wang) on reasonable request.

Acknowledgments

The authors would like to thank all doctors, nurses, technicians, and patients involved in this study for their dedication to the study.

Author Contributions

All authors made a significant contribution to the work reported, whether that is in the conception, study design, execution, acquisition of data, analysis and interpretation, or in all these areas; took part in drafting, revising or critically reviewing the article; gave final approval of the version to be published; have agreed on the journal to which the article has been submitted; and agree to be accountable for all aspects of the work.

Funding

The Joint Research Project of Liaoning Provincial Technology Plan [Applied Basic Research Program, 2023-JH2/101700312]; Zhanjiang Science and Technology Plan Project (2022A01160); The high-level talents scientific research start-up funds of the Affiliated Hospital of Guangdong Medical University (1007Z20220002).

Disclosure

The authors declare that the research was conducted in the absence of any commercial or financial relationships that could be construed as a potential conflict of interest.

References

1. Li F, Aljahdali IAM, Zhang R, Nastiuk KL, Krolewski JJ, Ling X. Kidney cancer biomarkers and targets for therapeutics: survivin (BIRC5), XIAP, MCL-1, HIF1α, HIF2α, NRF2, MDM2, MDM4, p53, KRAS and AKT in renal cell carcinoma. *J Exp Clin Cancer Res*. 2021;40(1):254. doi:10.1186/s13046-021-02026-1
2. Escudier B, Porta C, Schmidinger M, et al. Renal cell carcinoma: ESMO clinical practice guidelines for diagnosis, treatment and follow-up†. *Ann Oncol*. 2019;30(5):706–720. doi:10.1093/annonc/mdz056
3. Gray RE, Harris GT. Renal cell carcinoma: diagnosis and management. *Am Fam Physician*. 2019;99(3):179–184.
4. Perazella MA, Dreicer R, Rosner MH. Renal cell carcinoma for the nephrologist. *Kidney Int*. 2018;94(3):471–483. doi:10.1016/j.kint.2018.01.023
5. Bhatt JR, Finelli A. Landmarks in the diagnosis and treatment of renal cell carcinoma. *Nat Rev Urol*. 2014;11(9):517–525. doi:10.1038/nrurol.2014.194
6. Bai ZY, Peng LS, Li RQ, Peng X, Yang Z. STK4 is a prognostic biomarker correlated with immune infiltrates in clear cell renal cell carcinoma. *Aging*. 2023;15(20):11286–11297. doi:10.18632/aging.205127
7. Matuszczak M, Kiljańczyk A, Salagierski M. Surgical approach in metastatic renal cell carcinoma: a literature review. *Cancers*. 2023;15(6):1804. doi:10.3390/cancers15061804
8. Andrejeva G, Capoccia BJ, Hiebsch RR, et al. Novel SIRPα antibodies that induce single-agent phagocytosis of tumor cells while preserving T cells. *J Immunol*. 2021;206(4):712–721. doi:10.4049/jimmunol.2001019
9. Ring NG, Herndler-Brandstetter D, Weiskopf K, et al. Anti-SIRPα antibody immunotherapy enhances neutrophil and macrophage antitumor activity. *Proc Natl Acad Sci USA*. 2017;114(49):E10578–e10585. doi:10.1073/pnas.1710877114
10. Yanagita T, Murata Y, Tanaka D, et al. Anti-SIRPα antibodies as a potential new tool for cancer immunotherapy. *JCI Insight*. 2017;2(1):e89140. doi:10.1172/jci.insight.89140
11. Hussell T, Bell TJ. Alveolar macrophages: plasticity in a tissue-specific context. *Nat Rev Immunol*. 2014;14(2):81–93. doi:10.1038/nri3600
12. Li Z, Sun C, Wang F, et al. Molecular mechanisms governing circulating immune cell heterogeneity across different species revealed by single-cell sequencing. *Clin Transl Med*. 2022;12(1):e689. doi:10.1002/ctm2.689
13. Liu X, Xu J, Zhang B, et al. The reciprocal regulation between host tissue and immune cells in pancreatic ductal adenocarcinoma: new insights and therapeutic implications. *Mol Cancer*. 2019;18(1):184. doi:10.1186/s12943-019-1117-9
14. Zhai K, Huang Z, Huang Q, et al. Pharmacological inhibition of BACE1 suppresses glioblastoma growth by stimulating macrophage phagocytosis of tumor cells. *Nat Cancer*. 2021;2(11):1136–1151. doi:10.1038/s43018-021-00267-9
15. Tang PM, Nikolic-Paterson DJ, Lan HY. Macrophages: versatile players in renal inflammation and fibrosis. *Nat Rev Nephrol*. 2019;15(3):144–158. doi:10.1038/s41581-019-0110-2
16. Terashima Y, Toda E, Itakura M, et al. Targeting FROUNT with disulfiram suppresses macrophage accumulation and its tumor-promoting properties. *Nat Commun*. 2020;11(1):609. doi:10.1038/s41467-020-14338-5
17. Kourtzelis I, Li X, Mitroulis I, et al. DEL-1 promotes macrophage efferocytosis and clearance of inflammation. *Nat Immunol*. 2019;20(1):40–49. doi:10.1038/s41590-018-0249-1
18. Cioni B, Zaalberg A, van Beijnum JR, et al. Androgen receptor signalling in macrophages promotes TREM-1-mediated prostate cancer cell line migration and invasion. *Nat Commun*. 2020;11(1):4498. doi:10.1038/s41467-020-18313-y
19. Huffaker TB, Ekiz HA, Barba C, et al. A Stat1 bound enhancer promotes Nampt expression and function within tumor associated macrophages. *Nat Commun*. 2021;12(1):2620. doi:10.1038/s41467-021-22923-5
20. Zhou J, Tang Z, Gao S, Li C, Feng Y, Zhou X. Tumor-associated macrophages: recent insights and therapies. *Front Oncol*. 2020;10:188. doi:10.3389/fonc.2020.00188
21. Xiang X, Wang J, Lu D, Xu X. Targeting tumor-associated macrophages to synergize tumor immunotherapy. *Signal Transduct Target Ther*. 2021;6(1):75. doi:10.1038/s41392-021-00484-9
22. Vergadi E, Ieronymaki E, Lyroni K, Vaporidi K, Tsatsanis C. Akt signaling pathway in macrophage activation and M1/M2 polarization. *J Immunol*. 2017;198(3):1006–1014. doi:10.4049/jimmunol.1601515
23. Wu X, Chen H, Wang Y, Gu Y. Akt2 affects periodontal inflammation via altering the M1/M2 ratio. *J Dent Res*. 2020;99(5):577–587. doi:10.1177/0022034520910127
24. Pinjusic K, Dubey OA, Egorova O, et al. Activin-A impairs CD8 T cell-mediated immunity and immune checkpoint therapy response in melanoma. *J Immunother Cancer*. 2022;10(5):e004533. doi:10.1136/jitc-2022-004533
25. Sanmamed MF, Nie X, Desai SS, et al. A burned-out CD8(+) T-cell subset expands in the tumor microenvironment and curbs cancer immunotherapy. *Cancer Discov*. 2021;11(7):1700–1715. doi:10.1158/2159-8290.Cd-20-0962
26. El-Khoueiry AB, Sangro B, Yau T, et al. Nivolumab in patients with advanced hepatocellular carcinoma (CheckMate 040): an open-label, non-comparative, Phase 1/2 dose escalation and expansion trial. *Lancet*. 2017;389(10088):2492–2502. doi:10.1016/s0140-6736(17)31046-2
27. Nath PR, Pal-Nath D, Mandal A, Cam MC, Schwartz AL, Roberts DD. Natural killer cell recruitment and activation are regulated by CD47 expression in the tumor microenvironment. *Cancer Immunol Res*. 2019;7(9):1547–1561. doi:10.1158/2326-6066.cir-18-0367
28. Burt BM, Rodig SJ, Tilleman TR, Elbardissi AW, Bueno R, Sugarbaker DJ. Circulating and tumor-infiltrating myeloid cells predict survival in human pleural mesothelioma. *Cancer*. 2011;117(22):5234–5244. doi:10.1002/cncr.26143
29. Tang Y, Tian W, Zheng S, et al. Dissection of FOXO1-induced LYPLAL1-DT impeding triple-negative breast cancer progression via mediating hnRNPK/β-catenin complex. *Research*. 2023;6:0289. doi:10.34133/research.0289
30. Wu S, Lu J, Zhu H, et al. A novel axis of circKIF4A-miR-637-STAT3 promotes brain metastasis in triple-negative breast cancer. *Cancer Lett*. 2024;581:216508. doi:10.1016/j.canlet.2023.216508
31. Gao Z, Jiang J, Hou L, Zhang B. Dysregulation of MiR-144-5p/RNF187 axis contributes to the progression of colorectal cancer. *J Transl Int Med*. 2022;10(1):65–75. doi:10.2478/jtim-2021-0043
32. Zhao SJ, Kong FQ, Jie J, et al. Macrophage MSR1 promotes BMSC osteogenic differentiation and M2-like polarization by activating PI3K/AKT/GSK3β/β-catenin pathway. *Theranostics*. 2020;10(1):17–35. doi:10.7150/thno.36930
33. Zhao S, Mi Y, Guan B, et al. Tumor-derived exosomal miR-934 induces macrophage M2 polarization to promote liver metastasis of colorectal cancer. *J hematol oncol*. 2020;13(1):156. doi:10.1186/s13045-020-00991-2

34. Milella M, Rutigliano M, Pandolfo SD, et al. The metabolic landscape of cancer stem cells: insights and implications for therapy. *Cells*. 2025;14 (10):717. doi:10.3390/cells14100717
35. Arranz A, Doxaki C, Vergadi E, et al. Akt1 and Akt2 protein kinases differentially contribute to macrophage polarization. *Proc Natl Acad Sci USA*. 2012;109(24):9517–9522. doi:10.1073/pnas.1119038109
36. Wu X, Wang Y, Chen H, Wang Y, Gu Y. Phosphatase and tensin homologue determine inflammatory status by differentially regulating the expression of Akt1 and Akt2 in macrophage alternative polarization of periodontitis. *J Clin Periodontol*. 2023;50(2):220–231. doi:10.1111/jcpe.13730
37. Liu Y, Wang Y, Yang Y, et al. Emerging phagocytosis checkpoints in cancer immunotherapy. *Signal Transduct Target Ther*. 2023;8(1):104. doi:10.1038/s41392-023-01365-z
38. van Duijn A, SH VDB, Scheeren FA. CD47/SIRPα axis: bridging innate and adaptive immunity. *J Immunother Cancer*. 2022;10(7):e004589. doi:10.1136/jitc-2022-004589
39. Maute R, Xu J, Weissman IL. CD47-SIRPα-targeted therapeutics: status and prospects. *Immuno-Oncol Technol*. 2022;13:100070. doi:10.1016/j.iotech.2022.100070
40. Qu T, Li B, Wang Y. Targeting CD47/SIRPα as a therapeutic strategy, where we are and where we are headed. *Biomarker Res* 2022;10(1):20. doi:10.1186/s40364-022-00373-5
41. Dou L, Lu E, Tian D, Li F, Deng L, Zhang Y. Adrenomedullin induces cisplatin chemoresistance in ovarian cancer through reprogramming of glucose metabolism. *J Transl Int Med*. 2023;11(2):169–177. doi:10.2478/jtim-2023-0091
42. Wculek SK, Cueto FJ, Mujal AM, Melero I, Krummel MF, Sancho D. Dendritic cells in cancer immunology and immunotherapy. *Nat Rev Immunol*. 2020;20(1):7–24. doi:10.1038/s41577-019-0210-z